THE SPREADING RATE DEPENDENCE OF THREE-DIMENSIONAL MID-OCEAN RIDGE GRAVITY STRUCTURE

Jian Lin & Jason Phipps Morgan

Reprinted from

Geophysical Research Letters

Volume 19, Number 1, January 3, 1992

GEOPHYSICAL RESEARCH LETTERS, VOL. 19, NO. 1, PAGES 13-16, JANUARY 3, 1992

THE SPREADING RATE DEPENDENCE OF THREE-DIMENSIONAL MID-OCEAN RIDGE GRAVITY STRUCTURE

Jian Lin
Woods Hole Oceanographic Institution

Jason Phipps Morgan
Scripps Institution of Oceanography

Abstract. We analyze over 1300 km of high resolution along-axis gravity profiles at ridges with half-spreading rates ranging from 1.2 to 5.5 cm/yr. The results show consistently higher along-axis gradients of mantle Bouguer anomaly at the slow-spreading Mid-Atlantic Ridge (MAR) (0.3-1.2 mgal/km) than at the intermediate- to fast-spreading Cocos-Nazca Ridge and East Pacific Rise (EPR) (0.1-0.2 mgal/km). The regional peak-to-trough amplitude of mantle Bouguer anomaly is also greater along the MAR (30-60 mgal) than the Cocos-Nazca Ridge and the EPR (10-20 mgal). With increasing spreading rate, the regional peak-to-trough amplitude of axial seafloor depth decreases from 1000-1700 m to 200-700 m. 3-D numerical experiments suggest that mantle contributions to the gravity can be significant only near large-offset transforms. At the more commonly observed non-transform offsets, gravity anomalies will reflect crustal thickness variations.

The along-axis gravity data thus indicate that the amplitude of along-axis crustal thickness variation decreases with increasing spreading rate. We propose that this spreading rate dependent crustal accretion style may originate in the mantle: finite-amplitude mantle upwelling is intrinsically plume-like (3-D) beneath a slow-spreading ridge but more sheet-like (2-D) beneath a fast-spreading ridge. Such a transition in mantle upwelling may occur if the relative importance of passive upwelling over buoyant upwelling increases with increasing spreading rate. Small amplitude 3-D upwellings may occur at a fast-spreading ridge, but their effects on crustal thickness variations will be significantly reduced by along-axis melt flows along a persistent low-viscosity crustal magma chamber. In contrast, the large crustal thickness variations due to 3-D mantle upwellings will be maintained at a slow-spreading ridge because less along-axis melt flows can occur in the colder and more rigid crust there.

Data Analysis and Results

In the past few years, a number of geophysical surveys have mapped the gravity field over portions of mid-ocean ridges in dense two-dimensional grids. To reveal more subtle density variations beneath the seafloor, these studies reduced gravity data to mantle Bouguer anomalies (MBA) by removing the gravity effects of seafloor topography, as well as the effects of the crust-mantle interface assuming a 6-km thick uniform crust (Figure 1a, *Lin et al.*, 1990; 1b, *Phipps Morgan and Kleinrock*, 1991; 1c, *Madsen et al.*, 1990).

To search for systematic along-axis variations in the gravity and bathymetry, we extracted more than 1300 km of along-axis MBA and seafloor depth profiles from data of Figure 1, and additional data from the MAR at 31-34°S [*Kuo and Forsyth*, 1988], 25°-26°30'S [*Blackman and Forsyth*, 1991], and 22°30'-23°30'N [*Morris and Detrick*, 1991]. The profiles in Figure 2 show a number of first-order features that are related to ridge segments. The positive MBA is typically greater, and the seafloor is deeper, near first- and second-order ridge-axis discontinuities such as transforms, overlapping spreading centers (OSC), and non-transform offsets. The seafloor depth profiles at all ridges "mirror" the MBA profiles.

We define the half-segment amplitude as the difference in MBA from the segment mid-point to a distal end. Along the MAR, half-segment MBA amplitudes correlate positively with half-segment lengths (Figure 3a). The half-segment anomalies at the MAR (5-50 mgal) are consistently greater than those of the Cocos-Nazca Ridge and the EPR (5-20 mgal), although only a few data points are available for intermediate- and fast-spreading rates. To better quantify spreading-rate effects, we normalize the half-segment MBA amplitude by half-segment length. Results in Figure 3b show a range of 0.3-1.2 mgal/km for the MAR spreading segments. These values are consistently greater than those of the Cocos-Nazca Ridge and the EPR (0.1-0.2 mgal/km). Among MAR segments, greater along-axis changes occur near large-offset transforms - gradients near the Cox, Rio Grande, Kane, and Atlantis fracture zones (FZ) all exceed 0.7 mgal/km.

Regional amplitude is another measure of along-axis variability. We define regional amplitude as the peak-to-trough variation (4σ) of each regional profile (Figure 4). Results in Figure 3c show that the regional MBA amplitude is consistently greater at the MAR (30-60 mgal) than at the Cocos-Nazca Ridge and the EPR (10-20 mgal). Similarly, the regional amplitude of axial seafloor depth is greater at the MAR (1000-1700 m) than at the Cocos-Nazca Ridge and the EPR (200-700 m) (Figure 3d). Thus both along-axis MBA gradients and regional amplitudes suggest strong along-axis variations in the density structure of slow-spreading ridges; these variations decrease with increasing spreading rate.

Gravity Models

We have estimated specific mantle and crustal contributions to the MAR gravity. Based on a passive upwelling model [*Phipps Morgan and Forsyth*, 1988], we show that mantle effects due to thermal expansion predict only 1/3 of the MBA at the Atlantis transform and very little anomaly at small offsets (Figure 5). The combined effects of mantle thermal expansion and melt extraction can explain about 1/2 of the Atlantis transform anomalies (Figure 5); but the predicted anomaly is still too small to explain that observed at non-transform offsets. Recent 3-D numerical studies of buoyant upwelling also predict little mantle anomaly at small ridge offsets [*Parmentier and Phipps Morgan*, 1990; *Sparks and Parmentier*, 1990]. These studies show that significant buoyant upwelling and melting can develop in a low-viscosity mantle without producing large direct gravity signals.

Thus the large anomalies at MAR non-transform offsets will reflect crustal density structure. The residual anomaly at the MAR, if due solely to crustal thickness variation, is equivalent to nearly 50% reduction in the crustal thickness from segment center to distal ends [*Kuo and Forsyth*, 1988; *Lin et al.*, 1990]. In contrast, the EPR anomalies (Figure 1c,d) imply little along-axis crustal thickness variation.

We propose that the contrasting crustal accretion styles at fast- and slow-spreading ridges may originate in the mantle: mantle upwelling may have a 3-D plume structure beneath a slow-spreading ridge but a 2-D sheet structure beneath a fast-spreading ridge (Figure 6). The upwelling magnitude of a buoyant plume can be characterized by the terminal velocity of

Paper number 91GL03041
0094-8534/92/91GL-03041$03.00

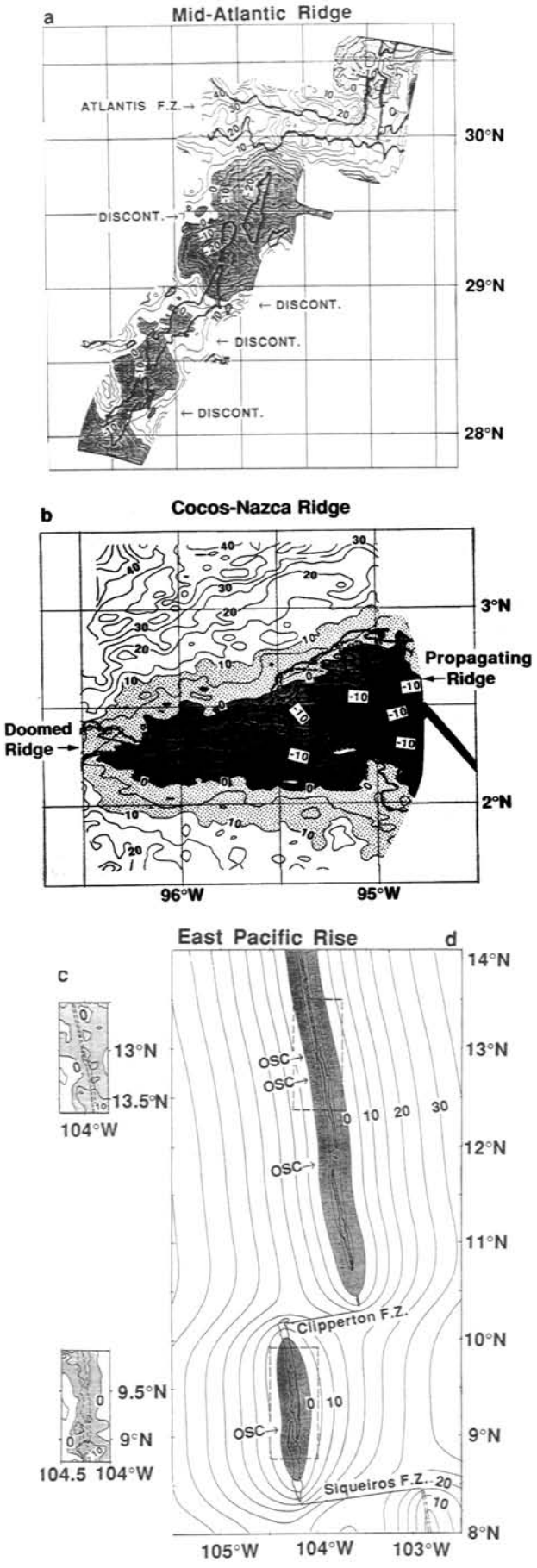

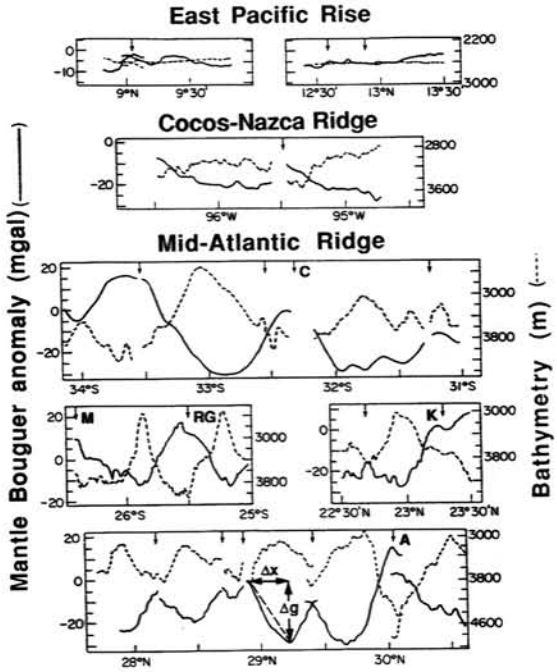

Fig. 2. Along-axis profiles of seafloor depth (dashed lines) and MBA (solid lines). Arrows mark first- and second-order ridge-axis discontinuities: transforms (labeled), overlapping spreading centers, and non-transform offsets. C-Cox; M-Moore; RG-Rio Grande; K-Kane; A-Atlantis.

a buoyant sphere, $W_b=(4/15)(\Delta\rho g a^2/\mu)$, where $\Delta\rho$ is the density deficit of the sphere relative to surrounding mantle, a is the sphere radius, and μ is the common viscosity of the sphere and the surrounding mantle [p.236, *Batchelor*, 1967]. For $\mu=10^{19}$ Pa-s, a=20 km, and $\Delta\rho$=0.01 Mg/m^3 (corresponding to density reduction after 5% melt extraction [*Oxburgh and Parmentier*, 1977]), the predicted W_b is of the same magnitude as the passive upwelling velocity, $W_p=(2/\pi)U$, at a ridge of half-spreading rate U=3 cm/yr. Such plume-like upwelling may result in greater melt production (Dick, 1989) and thicker crust beneath segment mid-points at a slow-spreading ridge (Figure 6). However, the direct mantle gravity signal from such a buoyant sphere is only a few mgals.

The above analysis suggests that as the spreading rate increases the relative importance of buoyant upwelling W_b/W_p

Fig. 1. (a-c) Mantle Bouguer anomaly (MBA) maps contoured at 5 mgal intervals. Zero level is arbitrary. The MBA maps were generated by subtracting from the free-air anomaly the attraction of seafloor topography and the attraction of relief on the crust-mantle interface assuming a uniform 6-km thick crust. Densities of 1.03, 2.7, and 3.3 Mg/m^3 were assumed for sea water, crust, and mantle respectively. Bathymetric contours are shown to outline the position of axial valleys in the MAR (3,200 m) and the Cocos-Nazca Ridge (3,000 and 3,200 m), and axial highs in the EPR (2,700 m). (d) Predicted gravity pattern at the EPR due to mantle thermal expansion for a model of solely passive mantle upwelling. We calculated a 3-D mantle temperature model assuming 0°C at the seafloor and 1350°C at a depth of 100 km, and converted temperatures to density changes by multiplying a thermal expansion coefficient of 3.4 x 10^{-5} °C^{-1}. Sea level gravity was then found from these density anomalies.

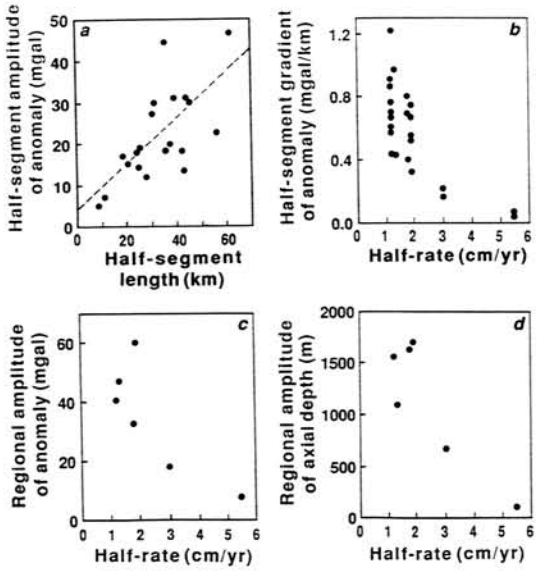

Fig. 3. (a) Plot of half-segment MBA amplitude Δg against half-segment length Δx for 20 half-segments along the MAR. (Definition of Δg is illustrated in the bottom panel of Figure 2.) The dashed line shows a best-fit linear relationship. (b) Plot of half-segment MBA gradient $\Delta g/\Delta x$ against half-spreading rate. $\Delta g/\Delta x$ is the mean along-axis gradient of the MBA within a half-segment. (c) Plot of regional amplitude of MBA against half-spreading rate. The regional amplitude is defined as the peak-to-trough variation (4σ) of a regional profile (see calculations of Figure 4). (c) Plot of regional amplitude of the axial seafloor depth against half-spreading rate.

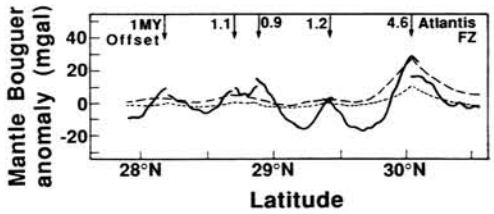

Fig. 5. Comparison of predicted mantle gravity effects (dashed lines) with observed MBA (solid lines). Arrows show ridge-axis discontinuities; numbers beneath the arrows show ridge-offset lengths in terms of age (in million years). The short dashed line shows mantle effects due to mantle thermal expansion. The long dashed line shows combined effects of thermal expansion and melt extraction. (Melt extraction reduces the density of melt-depleted mantle because the residual mantle has a lower Fe/Mg ratio [*Oxburgh and Parmentier*, 1977].) All calculations assume high viscosity (>10^{21} Pa-s) mantle, in which the upwelling is driven solely by plate separation and the buoyant component is minimized.

diminishes and along-axis variations in magma supply may become more subdued (Figure 6). A persistent crustal magma chamber, which exists only at fast-spreading ridges [*Detrick et al.*, 1987; *Macdonald et al*, 1988], may also play an important role in smoothing the crust. The low-viscosity crust inside the magma chamber of a fast-spreading ridge may not be able to support stresses due to large along-axis crustal thickness variations. Therefore if small amplitude 3-D upwellings occur at a fast-spreading ridge, their effects on crustal thickness variations will be significantly reduced by along-axis magma chamber melt flows. This may also help to explain the observed small gravity gradients along the Cocos-Nazca Ridge and the EPR (Figure 3b). In contrast, the large crustal thickness variations due to 3-D mantle upwellings will be maintained at a slow-spreading ridge because less along-axis melt flows can occur in the colder and more rigid crust there.

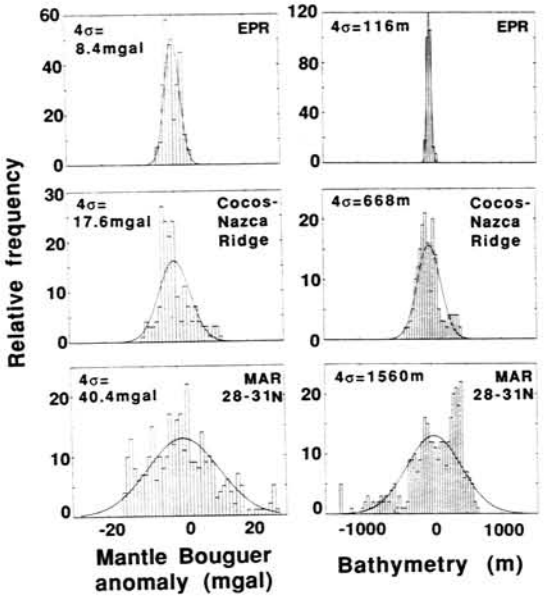

Fig.4. Histograms of along-axis MBA (left) and seafloor depth (right) for three of the six regions studied. Discrete points are sampled along regional ridge-axis profiles at a 1-km interval. Solid curves show best-fit models assuming a Gaussian normal distribution. σ is the standard deviation: 95% of points fall within -2σ to $+2\sigma$. Regional amplitude (peak-to-trough variation) is measured by 4σ.

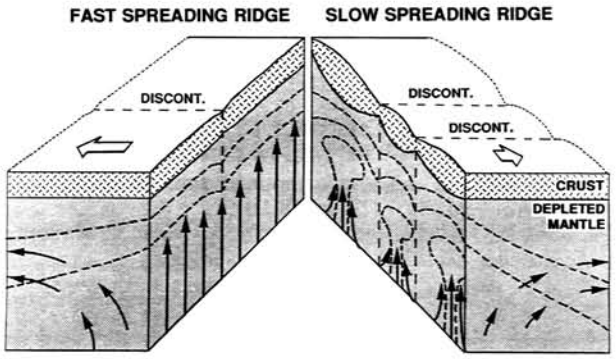

Fig. 6. A spreading-rate dependent model of crustal accretion and mantle upwelling that is consistent with the observed gravity and bathymetry. Solid arrows show mantle flow directions. Open arrows show plate motion vectors. Dashed lines in the mantle show isotherms. Gravity analyses indicate that the crustal density structure is relatively uniform at a fast-spreading ridge (left). At a slow-spreading ridge, however, the crustal thickness may vary continuously along a spreading segment, even if the segment is bounded by non-transform offsets (right). Such contrasting crustal accretion patterns may result from a dominantly plume-like upwelling and melting beneath a slow-spreading ridge and sheet-like mantle upwelling and melting beneath a fast-spreading ridge. Smaller amplitude 3-D upwellings may still occur at a fast-spreading ridge, but their effects on crustal thickness variations will be further reduced by along-axis melt flows along a persistent low-viscosity crustal magma chamber.

Besides the above first-order spreading-rate dependent features, inter-segment variability occurs along all ridges. For example, the positive correlation of MBA with segment length (Figure 3a) suggests that magma supply is greater at longer MAR spreading segments. Figure 3a further suggests that even for similar spreading-rate and segment-length, the MBA may differ by a factor of 3-4. Whether such inter-segment differences reflect variations in mantle melt supply or in crustal magma chamber structure awaits further investigations.

Conclusions

Our analyses of ridge-axis gravity data reveal strong spreading-rate dependent variability. Along-axis mantle Bouguer anomaly gradients at the MAR vary from 0.3 to 1.2 mgal/km; these values are systematically greater than those found on the Cocos-Nazca Ridge and the EPR (0.1-0.2 mgal/km). The regional amplitude of the mantle Bouguer anomaly is also greater along the MAR (30-60 mgal) than the Cocos-Nazca Ridge and the EPR (10-20 mgal). As the spreading rate increases, the regional amplitude in axial seafloor depth decreases from 1000-1700 m to 200-700 m.

The MAR gravity structure clearly indicates that crustal accretion at this slow-spreading ridge is focused at discrete centers. This accretion pattern implies a plume-like mantle upwelling and melting pattern as well. The most direct gravity effect of such plume-like upwelling is along-axis crustal thickness variations. The Cocos-Nazca Ridge and EPR data suggest that upwelling and melting distribution may become more sheet-like as the spreading rate increases. Finally, the observed high gravity gradients along the MAR and low gradients along the EPR imply that the effective crustal viscosity of a ridge increases with decreasing spreading rate. As a result, large crustal thickness variations will be maintained only at slow-spreading ridges.

Acknowledgments. We are indebted to John Madsen for permission to reproduce the EPR data. We thank Marty Kleinrock, Debbi Smith, Ross Stein, and two anonymous reviewers for constructive reviews. This work was supported by NSF and ONR. WHOI contribution number 7319.

References

Batchelor, G.K., *An introduction to fluid dynamics*, 615 pp. Cambridge Univ. Press, Cambridge, 1967.

Blackman, D.K., and D.W. Forsyth, Isostatic compensation of tectonic features of the Mid-Atlantic Ridge: 25-27°30'S, *J. Geophys. Res.*, *96*, 11,741-11,758, 1991.

Detrick, R.S., P. Buhl, E. Vera, J. Mutter, J. Orcutt, J. Madsen, and T. Brocher, Multi-channel seismic imaging of a crustal magma chamber along the East Pacific Rise, *Nature, 326*, 35-41, 1987.

Dick, H.J.B., Abyssal peridotites, very slow spreading ridges and ocean ridge magmatism, *Geological Society Special Publication, 42*, 71-105, 1989.

Kuo, B.Y., and D.W. Forsyth, Gravity anomalies of the ridge-transform system in the South Atlantic between 31 and 34.5°S: Upwelling centers and variations in crustal thickness, *Marine Geophys. Res., 10*, 205–232, 1988.

Lin, J., G.M. Purdy, H. Schouten, J.–C. Sempere, and C. Zervas, Evidence from gravity data for focused magmatic accretion along the Mid-Atlantic Ridge, *Nature, 344*, 627-632, 1990.

Macdonald, K.C., P.J. Fox, L.J. Perram, M.F. Eisen, R.M. Hymon, S.P. Miller, S.M. Carbotte, M.-H. Cormier, and A.N. Shor, A new view of the mid-ocean ridge from the behavior of ridge-axis discontinuities, *Nature, 335*, 217-225, 1988.

Madsen, J., R.S. Detrick, J.C. Mutter, P. Buhl, and J.A. Orcutt, A two- and three-dimensional analysis of gravity anomalies associated with the East Pacific Rise at 9°N and 13°N, *J. Geophys. Res., 95*, 4967-4987, 1990.

Morris, E., and R. S. Detrick, Three-dimensional analysis of gravity anomalies in the MARK area, Mid-Atlantic Ridge 23°N, *J. Geophys. Res., 96*, 4355-4366, 1991.

Oxburgh, E.R., and E.M. Parmentier, Compositional and density stratification in oceanic lithosphere - causes and consequences, *J. Geol. Soc. Lond., 133*, 343–355, 1977.

Parmentier, E.M., and J. Phipps Morgan, Spreading-rate dependence of three-dimensional structure in oceanic spreading centers, *Nature, 348*, 325-328, 1990.

Phipps Morgan, J., and D.W. Forsyth, 3-D flow and temperature perturbations due to a transform offset: Effects on oceanic crustal and upper mantle structure, *J. Geophys. Res., 93*, 2955–2966, 1988.

Phipps Morgan, J., and M.C. Kleinrock, Transform zone migration: implications of bookshelf faulting at oceanic and Icelandic propagating ridges, *Tectonics,10*, 920-935, 1991.

Sparks, D.W., and E.M. Parmentier, Buoyant flow beneath ridge-transform systems and along-axis variations in gravity and crustal thickness (abstract), *Eos, 71*, 627, 1990.

Jian Lin, Department of Geology & Geophysics, Woods Hole Oceanographic Institution, Woods Hole, MA 02543.

Jason Phipps Morgan, Institute of Geophysics and Planetary Physics, Scripps Institution of Oceanography, La Jolla, CA 92093.

(Received: August 23, 1991;
accepted: October 22, 1991)